Integrated spatial and multimodal single-cell transcriptomics reveal patient-dependent cell heterogeneity in splenic marginal zone lymphoma

Juan Pablo Cerapio, Pauline Gravelle, Anne Quillet-mary, Carine Valle, Frederic Martins, Don-marc Franchini, Charlotte Syrykh, Pierre Brousset, Alexandra Traverse-glehen, Loic Ysebaert, et al.

Journal of Pathology
J Pathol August 2024; **263:** 442–453
Published online 3 June 2024 in Wiley Online Library
(wileyonlinelibrary.com) DOI: 10.1002/path.6296

ORIGINAL ARTICLE

Integrated spatial and multimodal single-cell transcriptomics reveal patient-dependent cell heterogeneity in splenic marginal zone lymphoma

Juan Pablo Cerapio[1,2,3†], Pauline Gravelle[1,2,3,4,5†], Anne Quillet-Mary[1,2,3,4], Carine Valle[1,2,3], Frederic Martins[6], Don-Marc Franchini[1,2,3,4,5], Charlotte Syrykh[1,5], Pierre Brousset[1,2,3,4,5], Alexandra Traverse-Glehen[7], Loic Ysebaert[1,2,3,4,5], Jean-Jacques Fournie[1,2,3,4] and Camille Laurent[1,2,3,4,5*]

[1] *Université de Toulouse, INSERM UMR1037, CNRS UMR5071, Université Toulouse III-Paul Sabatier, Centre de Recherches en Cancérologie de Toulouse, Toulouse, France*
[2] *Institut Universitaire du Cancer-Oncopole de Toulouse, Toulouse, France*
[3] *Laboratoire d'Excellence 'TOUCAN-2', Toulouse, France*
[4] *Institut Carnot Lymphome – ADREP CALYM, Paris, France*
[5] *Centre Hospitalier Universitaire, Toulouse, France*
[6] *Institut Maladies Metaboliques et Cardiovasculaires, INSERM UMR1297, Toulouse, France*
[7] *Pathology Department, Centre Hospitalier Universitaire Lyon-Sud, Hospices Civils, Lyon, France*

**Correspondence to: C Laurent, Département d'Anatomie et Cytologie Pathologiques, Institut Universitaire du Cancer Toulouse – Oncopole, 1 avenue Irène Joliot-Curie, 31059 Toulouse Cedex 9, France. E-mail: laurent.c@chu-toulouse.fr*

†These authors contributed equally to this work.

Abstract

Biological hallmarks of splenic marginal zone lymphoma (SMZL) remain poorly described. Herein, we performed in-depth SMZL characterization through multimodal single-cell analyses of paired blood/spleen samples. The 3'-single-cell RNA-sequencing, Cellular Indexing of Transcriptomes and Epitopes by sequencing, and 5'-V(D)J single-cell RNA-sequencing datasets were integrated to characterize SMZL transcriptome profiles, including B-cell receptor and T-cell receptor repertoires. Hyperexpanded B-cell clones in the spleen were at a memory-like stage, whereas recirculating tumor B-cells in blood encompassed multiple differentiation stages, indicating an unexpected desynchronization of the B-cell maturation program in SMZL cells. Spatial transcriptomics showed the enrichment of T-effector and T-follicular helper (T_{FH}) signatures in the nodular subtype of SMZL. This latter also exhibited gene-based cell–cell interactions suggestive of dynamic crosstalk between T_{FH} and cancer cells in transcriptomics, further substantiated by using imaging mass cytometry. Our findings provide a comprehensive high-resolution description of SMZL biological hallmarks and characterize, for the first time *in situ*, inter- and intra-patient heterogeneity at both transcriptomic and protein levels.

Keywords: multimodal omics; single-cell RNA-sequencing; spatial transcriptomics; lymphoma; microenvironment

Received 20 September 2023; Revised 22 December 2023; Accepted 17 April 2024

No conflicts of interest were declared.

Introduction

Marginal zone lymphomas (MZLs) are indolent chronic B-cell lymphomas comprising approximately 6% of all non-Hodgkin lymphomas. MZLs include three distinct entities: splenic MZL (SMZL), nodal MZL, and extranodal MZL of mucosa-associated lymphoid tissue [1,2]. Among them, SMZL is characterized by a proliferation of small lymphomatous B-cells infiltrating the spleen and bone marrow, and involving peripheral blood. The prognosis of SMZL is generally good, with median survival around 15 years; nevertheless, one-third of patients still have a poor outcome, with multiple relapses and possibly a progression or transformation into an aggressive lymphoma [3]. Therapeutic strategies for these entities are undergoing rapid evolution, with no standard treatment available [4,5]. Given the heterogeneity of clinical evolution, understanding the development and progression of SMZL is paramount.

The postulated origin of B-cells with IgM^{high} IgD^{low}, and CD27 phenotype is an antigen-experienced B-cell homing at the marginal zone (MZ) [3]. This zone surrounding secondary follicles is composed of B- and T-lymphocytes, dendritic cells/macrophages, and follicular

dendritic cells capturing and presenting blood-borne antigens to the MZ B-cells. Thus, MZ B-cells are continuously exposed to antigens, leading to B-cell receptor (BCR) engagement. The assumption that antigen recognition could play a role in the pathogenesis of SMZL is supported by the somatic hypermutation and biased repertoire of the *IGVH* gene, involving *IGVH*1-2*04 allele in approximately 30% of cases [6,7].

In addition, SMZL exhibits multiple mutations, but not unifying genomic alterations, that induce constitutive BCR, Toll-like receptor, NF-κB, and NOTCH signaling. Of note, most of these pathways are involved in normal MZ differentiation [8–13]. Recently, four molecular clusters in SMZL with two prominent genetic clusters termed NNK (representing 58% of cases, including mutated genes in NF-kB, NOTCH, and KLF2 modules) and DMT (32% of cases, with mutations in genes DNA damage response, MAPK, and Toll-like receptor modules), have been identified [12]. Finally, 30% of SMZL harbor chromosome 7q deletions, while gains of 3q, 12q, and 18q are less frequent.

Beyond the genetic lesions, the tumor microenvironment (TME) of SMZL remains poorly understood. A subset of SMZL shows an expansion of inflammatory T-cells [14], which suggests TME is distinct among SMZL patients with different outcomes. Although distinct histological patterns of SMZL have been reported [1,2,15], their relationship with TME remains to be investigated.

Single-cell RNA-sequencing (scRNA-seq) technologies are so far the most successful method for dissecting the cellular composition of malignant tissue and identifying the molecular markers of each subpopulation. However, characterizing the cellular and molecular heterogeneity of cancer samples *in situ* represents a major challenge. Here we performed multimodal scRNA-seq profiling by both 3' Cellular Indexing of Transcriptomes and Epitopes by sequencing (CITE-seq) and 5'-V(D)J-repertoire of paired blood and spleen samples from SMZL patients, further combined with both spatial transcriptomics and multispectral imaging analysis of the spleen samples. Our study revealed unexpected molecular hallmarks and novel cellular interactions that underlie the heterogeneous physiopathology of SMZL.

Materials and methods

Patient sample collection

SMZL samples were processed for cytogenetic studies and histopathological examination, including immunochemistry studies and 67 targeted genes sequenced by next-generation sequencing (see Supplementary materials and methods) [16]. The control spleen specimens were obtained from patients with a traumatic spleen injury. Clinical information is detailed in Supplementary materials and methods. All samples were collected at the Institut Universitaire du Cancer de Toulouse-Oncopole (IUCT-O) following standard ethical procedures (Declaration of Helsinki) and after obtaining written informed consent and approval by the Institutional Review Board (DC-2009-989 AC-2008-820).

Single-cell RNA-sequencing

After SMZL and healthy donor (HD) sample cell isolation (see Supplementary materials and methods), scRNA-seq libraries were prepared following the manufacturer's instructions (10x Genomics, Pleasanton, CA, USA), using Chromium Single Cell 3' (V3) and 5' (V1) Library & Gel Bead Kit and Chromium Controller Single-Cell Instrument (10x Genomics). Cell surface protein labeling was performed before single-cell 3'-library construction using 1 µg each of the following TotalSeq-B antibodies (Biolegend, San Diego, CA, USA): anti-CD274 (800234), anti-CD45RO (800238), anti-CD3 (800239), anti-CD19 (800241), anti-CD279 (800248), anti-TIGIT (800249), anti-CD45RA (800253), anti-CD4 (800255), anti-CD8a (800257), anti-CD14 (800258), anti-CD56 (800259), and anti-CD25 (800260). scRNA-seq data pre-processing and quality control are detailed in Supplementary materials and methods.

Spatial transcriptomics

Frozen sections of spleen samples were mounted on to Visium spatial slides, fixed using methanol, stained with H&E and digitized using an LSM 710 videomicroscope (Carl Zeiss Microscopy, München, Germany). Then, tissues were permeabilized on the slide and reverse transcription was performed *in situ*. Finally, second-strand synthesis, denaturation, DNA amplification, library construction, and sequencing were performed following the manufacturer's instructions (Visium Spatial Gene Expression Reagent Kits User Guide – Rev C, 10x Genomics).

Signature scores

Unless specified otherwise, the gene signatures were from MSigDB (https://www.gsea-msigdb.org/gsea/msigdb/collections.jsp) or published elsewhere [17]. Each signature was scored for every single cell or spatial spot using the Single-cell Signature-Scorer [18], then merged with cell or spot coordinates [uniform manifold approximation and projection (UMAP), Minimum Spanning Tree (MST), spatial transcriptomic (ST)], and visualized using Single-Cell Signature-Explorer [18], Multilayer-Viewer [19], or Spatial-Explorer [20] (open source software developed at CRCT, Toulouse, France).

ST-inlays

ST-inlays are scRNA-seq-derived numerical scores mapped on a microscopy image of H&E-stained tissue using the Single-Cell Spatial-Explorer software (https://github.com/FredPont/spatial), which represents signature scores of spatial spots as heatmaps with tunable scales (minimum, maximum, opacity) [20].

Reference differentiation trajectories, *ab extra* cell injection, classifications

To infer a trajectory of peripheral B-lymphocytes, the MST method was applied on the reference scRNA-seq dataset of normal peripheral B-lymphocytes ($n = 4{,}662$) [17,21]. In contrast, for mapping the trajectory of B-cells from spleen tissue, ANGLE was selected and applied on the reference scRNA-seq dataset of germinal center B-lymphocytes (B_{GC}) ($n = 21{,}905$) from HD tonsils [21,22]. Each of the above B-cell trajectories represented the reference development trajectory for peripheral B-lymphocytes and B_{GC}, respectively (detailed in Supplementary materials and methods). In addition, T-cells (CD8 T and γδ T) were also injected in their respective trajectories, as previously reported [19,23]. In this work, CD4 T-cells from HD [24] were used to stablish the reference trajectory.

Synchronized B-cell differentiation genes

The pseudo-temporal evolution of top genes associated with blood B-cell development was analyzed as described previously [25]. Among the 80 top genes associated with the peripheral B-cell differentiation trajectory, only those ($n = 38$) expressed by all samples were selected for expression analysis in each sample and visualized with cells and genes ordered by pseudo-time. The most correlated group of co-evolving genes was then analyzed for gene set enrichment across the entire MSIgDB by using AutoCompare_ZE [26] (open source software developed at CRCT, Toulouse, France; available at https://sites.google.com/site/fredsoftwares/products/autocompare-ze).

Gene-based ligand–receptor pair interactions

To investigate the gene expression-based ligand–receptor interactions, we used the Ligand-receptor Analysis Framework (LIANA) [27]. As reported, we applied the recommended workflow for 'consensus' analysis (https://github.com/saezlab/liana) and used as an input the annotated CD4 T- and B-cells of each SMZL spleen sample separately.

Imaging mass cytometry

The principle of the assay has been described previously [28]. Tissue labeling and data acquisition using the Hyperion Imaging System (Standard Biotools, San Francisco, CA, USA) were performed following the manufacturer's instructions, as described previously [29]. Further details are provided in Supplementary materials and methods.

Results

Integrative single-cell profiling of spleen and blood cells from SMZL patients

We generated 3'-CITE-seq and 5'-scRNA-seq V(D)J profiles of peripheral blood mononuclear cells and spleen cells from three patients with SMZL and two HD. In total, 90,556 cells passed quality control, were normalized, and integrated together into one so-called '3'-5' dataset'. 3'5'-UMAP validated the integration of the 3' and the 5' datasets as well as tissue origin (Figure 1A, and supplementary material, Figure S1a). Thus, the immune cells from each SMZL patient and those from HDs were clustered by main cell type, whereas tumor B-cells from each SMZL patient clustered distinctly by patient (Figure 1B). To identify the composition of these different areas, we performed unsupervised clustering and delineated 18 clusters (Figure 1C). These clusters were identified based on their differentially expressed genes and cell surface phenotypes (Figure 1D and supplementary material, Figure S1b,c). Consistent with BCR repertoire analyses, the private areas encompassed clusters of hyperexpanded tumor B-cell clones from each patient (supplementary material, Figure S1d).

The normal B-cells (*CD19*, *CD79A*, *CD79B*, *MS4A1*) from HD blood and spleen generated two clusters (clusters 13, 14). The HD control samples also encompassed a few plasmacytoid dendritic cells (*CLEC4C, IL3RA*) (cluster 18), scarce in SMZL samples. All samples together shared four T-cell clusters, including $CD4^+$ T, $CD8^+$ T, and a few γδ T-lymphocytes. These clusters delineated naïve T-cells (Tn) (*LEF1, TCF7, CCR7*) in cluster 4, central memory T-cells (T_{cm}) (*ANXA1*, *IL7R*, *KLRB1*, *LTB*) in cluster 6, effector T-cells [both effector memory (T_{em}) and effector memory $CD45RA^+$ (T_{emra})] (*CCL5*, *NKG7*, *GZMA*, *GZMK*) in cluster 7, and $CD3^+CD56^+$ NK-like T-cells (NKT) in cluster 15 (*GNLY*, *NKG7*, *IL32*, *PRF1*, *GZMA*). An adjacent cluster (cluster 10) of cytotoxic $CD3^-CD56^+$ non-T-cells corresponding to the NK cells was also identified. In addition, the myeloid cells comprised one macrophage cluster (*CD68*, *FCGR3A*, *FCER1G*, *TYROBP*) (cluster 12) and distinct monocyte clusters: monocytes (cluster 8) (*CD14*, *S100A8*, *S100A9*, *LYZ*), monocytes $CD16^+$ (cluster 11), classical dendritic cells-like (cluster 16), and active monocytes (cluster 17). Finally, each patient's blood and spleen samples comprised a large majority of cancer cells (SMZL1 in clusters 2 and 5; SMZL2 in cluster 1; SMZL3 in clusters 3 and 9).

Thereby, three major cell populations were identified in this dataset. Both circulating and splenic tumor SMZL B-cells corresponded to hyperexpanded lymphoma clones, which clustered together in a patient-specific manner. That indicated inter- and intra-patient heterogeneity of tumor B-cells in SMZL, while, in every patient, the immune microenvironment cells encompassed various proportions of T-cells and myeloid cells.

Multimodal analysis of SMZL tumor B-cells

Intra-tumor B-cell heterogeneity in B-cell lymphomas may result from divergent sub-clonal genetic evolution or cellular plasticity. Analyzing the 5'-V(D)J dataset, we first confirmed that the hyperexpanded B-cell clones expressed high IgM and low IgD chain

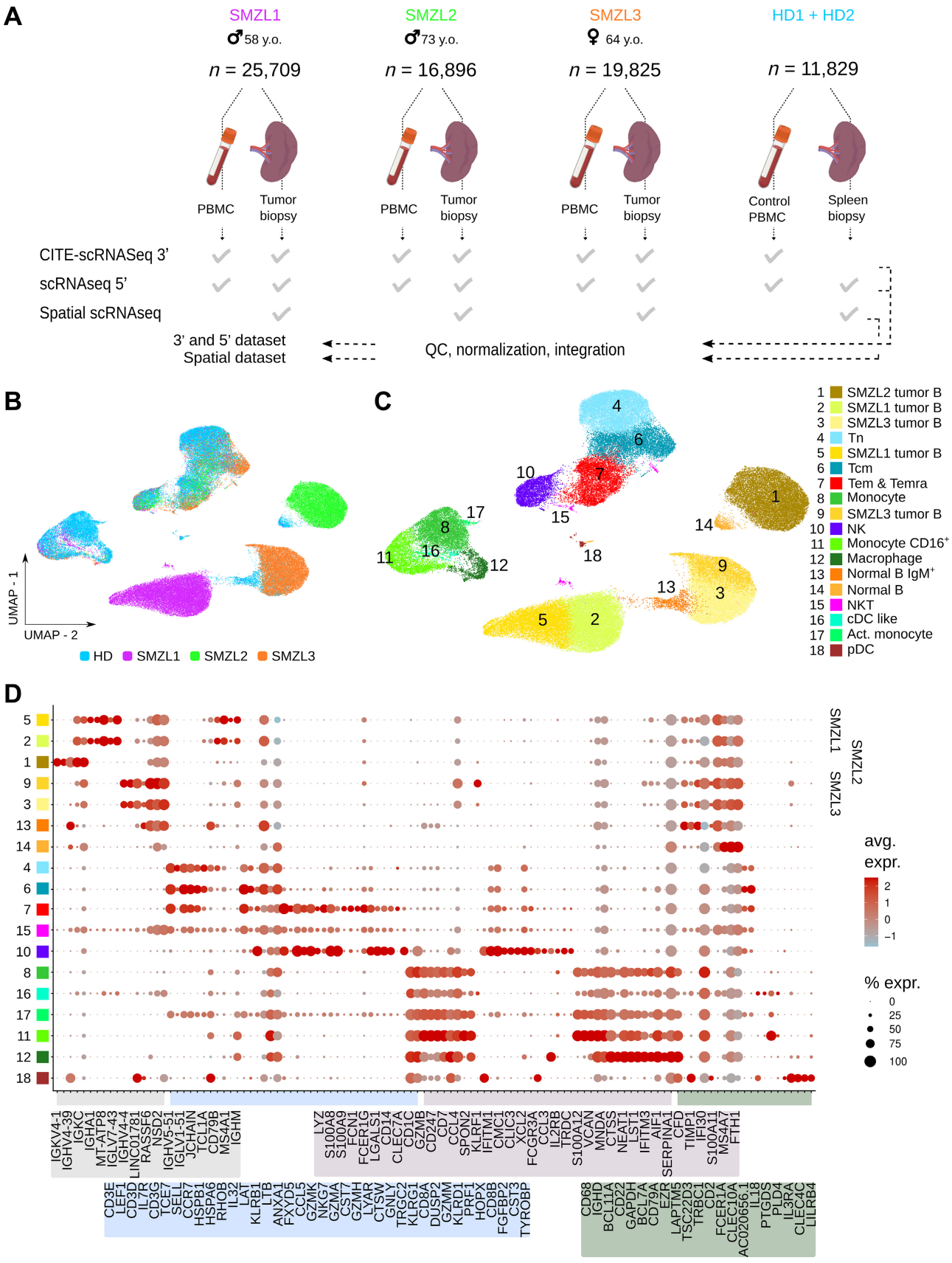

Figure 1. Multimodal single-cell transcriptomics of SMZL blood and spleen. (A) Sampling and analytic workflow. (B) 3'-5'-UMAP per patients and HD. (C) 3'-5'-UMAP per cluster. (D) Differentially expressed genes per cluster. The gene expression values are shown as the cluster's average (log2FC over all others) (color) and the cluster's percentage of expressing cells (bubble size). Same color key for (C) and (D).

encoded by selective use of Ig heavy: IGHV4-4D6-19J3/IGLV7-43J3C2 in SMZL1, IGHV4-39J5/IGKV4-1J4C in SMZL2, and IGHV5-51J4/IGLV1-51J2C2 in SMZL3 (Figure 2A). These results showed that hyperexpanded B-cell clones from each SMZL patient constituted distinct clusters in their single-cell transcriptomic dataset, primarily driven by their distinct IGH clonal sequences. Interestingly, these single IgM^{high} IgD^{low} B-cell clonotypes were prominent in both compartments, spleen, and circulating blood of each patient, suggesting the recirculation of tumor B-cells from spleen MZ.

To better characterize the heterogeneity of malignant B-cells, we next investigated the transcriptional states of the hyperexpanded B clones identified by the 5'-V(D)J sequence in each patient and excluded normal B-cells from all further analyses. We then investigated the temporal relationships among B-cell clusters by *ab extra* cell injection into reference differentiation trajectories (see Materials and methods and supplementary material, Figures S2 and S3). As expected, the physiological blood B-cell differentiation encompassed transitional B-cells (B_{trans}), naïve B-cells (B_n), IgM^+ memory B-cells ($B_{M\text{-}mem}$), classical memory B-cells ($B_{C\text{-}mem}$), and IgD^-CD27^- double negative (DN) B-cells comprising IgA-expressing DN ($B_{DN\ IgA}$) and IgM- and IgG-expressing DN ($B_{DN\ IgM\text{-}IgG}$) (see supplementary material, Figure S2). In contrast, the circular differentiation trajectory of B_{GC} ($n = 21{,}905$), revealed a GC zone entry ($B_{GC\ entry}$), dark zone (B_{DZ}), light zone (B_{LZ}), and GC zone exit ($B_{LZ\ exit}$). By projecting tumor splenic B-cells on the linear differentiation trajectory established for peripheral blood mononuclear cells, these cells mainly showed a commitment at the $B_{M\text{-}mem}$ stage (supplementary material, Figure S3). This indicated that a linear differentiation trajectory was not adapted to study the differentiation of splenic B-cells, which displayed a circular differentiation trajectory.

Then, to investigate the differentiation states of normal B-cells and SMZL hyperexpanded B-cell clones from blood and spleen (3'-5' dataset), they were injected on their respective reference trajectories (see Materials and methods). The peripheral B-cells from HD encompassed the six blood stages, whereas their B-splenocytes comprised predominantly $B_{LZ\ exit}$ cells, which also express markers of commitment to the $B_{M\text{-}mem}$ state (Figure 2B). Despite inter-patient variability, hyperexpanded tumor B-cell clones in the spleen were essentially on $B_{LZ\ exit}$, as the normal splenocytes. In contrast, their circulating counterpart presented multiple stages of differentiation (Figure 2B). Such findings showed that hyperexpanded B-cell SMZL clones are $B_{M\text{-}mem}$ cells like splenocytes ($B_{GC\text{-}LZ\text{-}like}$ according to reference trajectory) [22] and recirculated in blood SMZL patients with several differentiation phenotypes. This suggests a transcriptional desynchronization of B-cell maturation in SMZL, as observed in follicular lymphoma (FL) [25].

Thus, to further understand whether peripheral B-cell development programs were dissociated in SMZL, we analyzed the pattern of gene expression involved in the B-cell differentiation process. To this aim, the top-trajectory-associated genes of blood B-cells from HD were identified, ordered by differentiation stage, and presented in a heatmap (Figure 2C). Similar heatmaps were then generated for circulating B-cell samples from SMZL patients showing distinct expression patterns (Figure 2D).

Enrichment analyses indicated that these trajectory top-genes are notably involved in 'BCR signaling (KEGG)', 'B-cell activation (GO-BP)', or 'CD22-mediated BCR regulation (REACTOME)' (*MZB1*, *FOXP1*, *CD72*, *CD79B*, *IGHM IGHD*; $p =$ E-04), as well as 'Translation initiation complex formation (REACTOME)' (*RPS10*, *RPS24*; $p =$ 4E-03) and 'Leukocyte trans-endothelial migration' (KEGG) (*CXCR4, NCF1;* $p =$ 1.6e-02) (not shown). Notably, trajectory top-genes involved in BCR signaling (*MZB1*, *CD72*, *FOXP1*, *CD79B*, *IgHD*, *IgHM*) decreased concomitantly with differentiation in B-cells from HD, whereas they were dynamic and asynchronous in hyperexpanded B-cell clones from all SMZL patients (Figure 2E).

Finally, we investigated whether desynchronized B-cell programs were responsible for distinct signaling profiles in tumor B-cell clones. By scoring all MSIgDB gene signatures across the whole 3'-5' dataset and comparing the tumor (clusters 1, 2, 3, 5, 9) and normal (clusters 13, 14) B-cells, further molecular hallmarks of SMZL cancer cells were identified. Indeed, several signatures were significantly enriched in the tumor clusters relative to normal B-cells, such as BCR and NFKB signaling, and the KEGG cell cycle (Figure 2F). This signature profiling confirmed the inter-patient heterogeneity mentioned above, as exemplified by higher scores for BCR and NOTCH signaling in SMZL3 than SMZL1 and SMZL2, and for cell cycle in SMZL1 than SMZL2 and SMZL3.

Overall, the tumor B-cell clones were $B_{M\text{-}mem}$ cells, like splenocytes within the splenic tumor, but recirculated in the blood of SMZL patients with several stages of differentiation. In contrast to normal B-cells, hyperexpanded B-cell clones showed patient-specific gene expression profiles, enrichment of some cancer signaling pathways, and a transcriptional desynchronization of B-cell maturation programs. These features may participate in the intra-tumoral heterogeneity of malignant SMZL cells.

T-lymphocytes of SMZL TME

The next step of our analysis was to characterize the microenvironment cells from SMZL samples excluding the myeloid cells, whose paucity possibly reflected their under-sampling after thawing.

Based on integrative analyses from both transcriptomes (including epitope sequencing using CITE-seq) and UMAP clusters, all non-myeloid and non-B-cells were identified and classified as NK cells (cluster 10: $CD3^-$ cells), NKT (cluster 15: $CD3^+CD56^+$ cells), or T-lymphocytes (Figure 1C). Using the immunophenotype (3' CITE-seq data), the T-cell composition across the different stages of T-cell maturation: T_n, T_{cm}, T_{em}, and T_{emra}, was determined

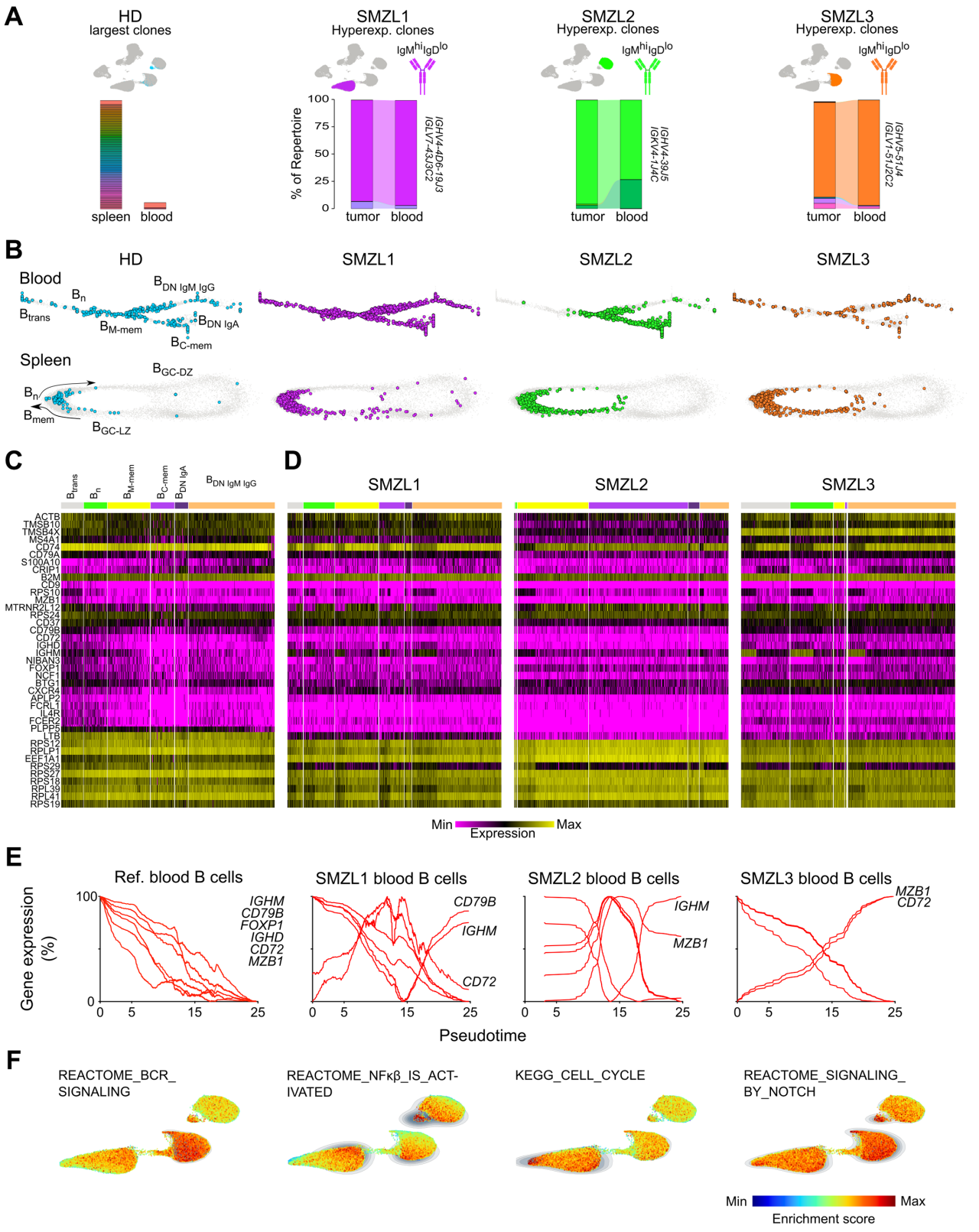

Figure 2. Multimodal characterization of SMZL tumor B-cells. (A) Sankey plots of the hyperexpanded B-cell clonotypes per patient; percentage of the B-cell repertoire. Upper insert: projection of the same clonotype in the 3'-5'-UMAP. The 30 largest (non-hyperexpanded) clones are shown for the HD samples. (B) Both blood and spleen, B-cells from HD (light blue) and tumor B-cell clones from the SMZL patients were injected into the normal blood B-cells (B, top) and human tonsil B_{GC} cells (B, bottom) reference trajectories (gray), respectively. (C) Expression of B-cell differentiation-associated top genes (left margin) in the (n = 4,662) reference blood B-cells from healthy adults [same cells as (B, top)], with genes and cell milestones, ordered based on evolution along pseudo-time. (D) Similar heatmaps (same genes and order) for blood B-cells from SMZL1 (n = 13,762 cells), SMZL2 (n = 8,326 cells), and SMZL3 (n = 10,849 cells). (E) Evolution along pseudo-time of representative B-cell differentiation genes in the specified cells. Expression is presented relative to the maximum expression. (F) Gene signatures significantly enriched (BH-corrected ZE $p < 10^{-7}$) in tumor B-cells relative to normal B-cells (clusters 13, 14), the enrichment scores for the specified signatures are shown only for B-cell clusters (clusters 1, 2, 3, 5, 9, 13, and 14).

for each sample (Figure 3A). The tumor infiltrates differed quantitatively between patients, but within patients, the T-cell subset composition of blood and spleen tumors was correlated (Pearson $r = 0.91$). Indeed, SMZL1 and SMZL2 tumors were weakly infiltrated, mostly by CD4 T_n (SMZL1) and CD8 T_{em} cells (SMZL2). By contrast, the spleen of SMZL3 was enriched in CD4 T_{cm} and γδ T_{em} cells. These findings were further verified by injecting T-cells into reference differentiation trajectories of the CD4 T- [24], CD8 T-, and γδ T-cell lineages [19,23] (see Supplementary materials and methods and supplementary material, Figure S4). The lymphoid environment of each sample also encompassed a few NK and NKT cells.

As shown in supplementary material, Figure S1, TCR-repertoire analyses revealed polyclonal T-cell populations with a moderate/high degree of sharing between blood and tumor (on average 10% of all TCR αβ clonotypes found in each patient were in both blood and tumor). More particularly, the T-cell clone sizes identified by the 5'-V(D)J data pinpointed recirculating tumor infiltrating lymphocyte (TIL) clonotypes (found in both tumor and blood) of large size (1–10% of the repertoire). In SMZL1, only three of the 24 largest TIL clones were recirculating (12%, including both CD4 and CD8 T-cells). In SMZL2 by contrast, six of eight (62%, all CD8 T-cells), and in SMZL3, six of the seven largest TIL clones (86%, all CD4 T-cells) recirculated (Figure 3B).

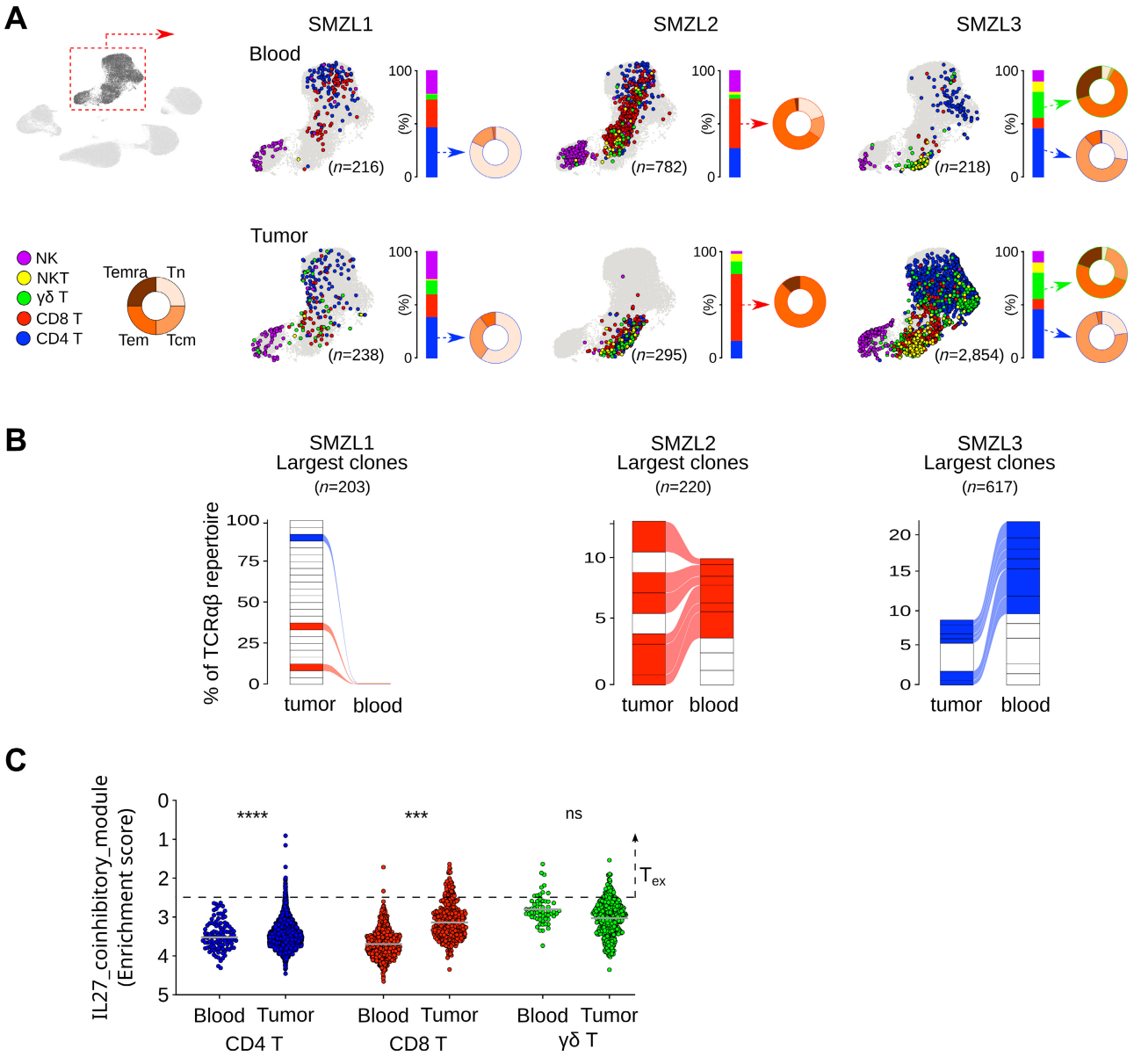

Figure 3. T- and NK cells infiltrating SMZL spleen and peripheral blood. (A) UMAP view of T- and NK cells from the integrated 3'-5' dataset (gate: upper insert) shown per sample and patient with subsets of lineage and percentage of each differentiation stage (legend). (B) Largest T-cell clones in the specified sample. (C) Distribution of single-cell scores for one T-cell exhaustion signature [45] in the specified cell groups (bars: group mean; dotted line: T exhausted (T_{ex}) positivity threshold).

In all patients, TIL that reached T_{em} and T_{emra} stages exhibited the most exhausted phenotype, as previously defined by multiple signatures [19]. In addition, CD4, CD8, displayed higher exhaustion signature scores in SMZL spleens, compared with their circulating T-cell counterparts (Figure 3C).

In summary, within patients, the composition of blood and tumor T-cell infiltrate was identical, but its content differed quantitatively across compartments. Between patients, heterogeneity was found in TILs with some tumors weakly infiltrated by TILs (SMZL1 and 2) identified as cold tumors, whereas other tumors were more inflamed with a microenvironment enriched in CD4 T-cells (SMZL3). In addition, some specific subpopulations of TIL in each tumor were characterized by immune escape features.

Spatial cartography of SMZL spleen

To explore the *in situ* organization of T-cells infiltrating the SMZL spleen, a biopsy from each SMZL splenic tissue and a control spleen were stained with H&E, imaged under a LSM 710 videomicroscope (Carl Zeiss Microscopy) (supplementary material, Figure S5a), and their spatial transcriptomes measured across 55 µm diameter spots by using Visium technology (10x Genomics). From these four samples, 7,116 spots of spatial transcriptomes were obtained, normalized together, and integrated as a single spatial dataset (supplementary material, Figure S5b,c).

First, public and in-house signatures for T- and B-cell subpopulations were scored for all samples together and inlayed across the spatial slides independently. As expected, T-cells were infiltrating all spleen tumors in a patient-associated manner. Validating the previous 3'–5' single-cell analysis, SMZL1 and SMZL2 were characterized by scarce T-cell infiltrates relative to SMZL3 and HD (Figure 4A). The $CD8^+$ cytotoxic population was randomly distributed within the tissue and was quite rare in all SMZL, as compared with HD (supplementary material, Figure S5d). Moreover, the SMZL1 and SMZL2 samples displayed very few T-follicular helper (T_{FH}) cells dispersed in the spleen; whereas in SMZL3, a T_{FH} population was organized in a structured manner surrounding B-cell nodules (Figure 4A) (depicted by a lighter H&E coloration in supplementary material, Figure S5a).

To further explore the molecular mechanism underlying the relationship between tumor and T-cells, putative gene-based ligand–receptor pair interactions were investigated on the 3'–5' dataset using LIANA (see Materials and methods). As shown in Figure 4B, strong predictive gene interactions between *CXCL13* and *CXCR5* expressed by CD4 T-cells and B-cells, respectively, were found in SMZL3, but absent in both SMZL1 and SMZL2 samples. Interestingly, CXCR5/CXCL13 signaling is known to promote chemotaxis and follicle formation in B- and T_{FH} cells and may contribute to the specific nodular architecture of SMZL3. Additional putative gene-based interactions between B- and T-cells were also identified in SMZLs, through the CD40L–CD40 axis, TNF superfamily, or BTLA and their receptors, such as TNFRSF14. Together, the predicted gene-based interactions, capable of promoting B-cell survival and proliferation, were more enriched in SMLZ3 than in SMZL1 and SMZL2.

Finally, these singular spatial patterns of tumor B- and T-cells were validated at the protein level in our SMZL patients and additional SMZLs ($n = 6$ in total), by using imaging mass cytometry (IMC, Hyperion imaging system, Standard Biotools) with a 34 antibody panel (supplementary material, Table S1) (see Materials and methods). As illustrated in Figure 4C, the FFPE samples from SMZL nodular subtypes exhibited a $CD4^+$ T-cell expansion into B nodules, whereas most $CD8^+$ T-cells lay in the inter-nodular area. In addition, nearly all peri- or inter-nodular $CD4^+$T-cells were positive for the CD45RO and PD-1 markers associated with the T_{em} differentiation and T_{FH} phenotype, respectively (Figure 4D). To further investigate the spatial proximity between tumor B-cells and T-cells, the distance among cells was calculated on tissue using IMC data (supplementary material, Figure S6a). We found that $CD4^+PD1^+$ T-cells were more likely to be found in close proximity to tumor B-cells as compared with $CD8^+$ T-cells as well as $PD1^-CD4^+$ T-cells. This proximity facilitates functional interactions between T_{FH} and tumor B-cells. We next quantified the number of $PD1^+CD4^+$ T-cells and Ki-67^+ tumor B-cells in nodule and diffuse areas of SMZLs and found a significant positive correlation between high tumor proliferation rate and T_{FH}-rich zones ($r = 0.72$; $p = 0.01$) in tumor nodules only (supplementary material, Figure S6b). Together, these findings validated, at the protein level, the previous multimodal transcriptomic findings and suggested a pro-survival interaction between T_{FH} and B-cells in SMZL nodular subtypes.

Discussion

Our integrative multimodal study represents the first *in situ* characterization at both transcriptomic [a total of 19 single-cell transcriptome datasets of blood and spleen paired samples from 3'CITE-seq ($n = 7$), 5'-V(D)J ($n = 8$), and spatial transcriptomics ($n = 4$) of three SMZL patients and two HD (see Figure 1A)] and protein (seven IMC samples) levels of inter- and intra-patient cell heterogeneity. For each SMZL patient, it identified the major tumor B-cell clones invading both spleen and blood. Despite harboring the same Ig phenotype (IgM^+ IgD^+ heavy chains and common light chain), these hyperexpanded clones surprisingly lack a specific developmental blockade and can simultaneously present successive stages of differentiation. Transcriptome analysis of 74,259 single cells showed that TMEs of SMZL also varied across patients, but each patient showed consistent T-cell repertoires in the blood and spleen, suggesting TILs recirculate as well in SMZL. This finding implies that the immune response can be

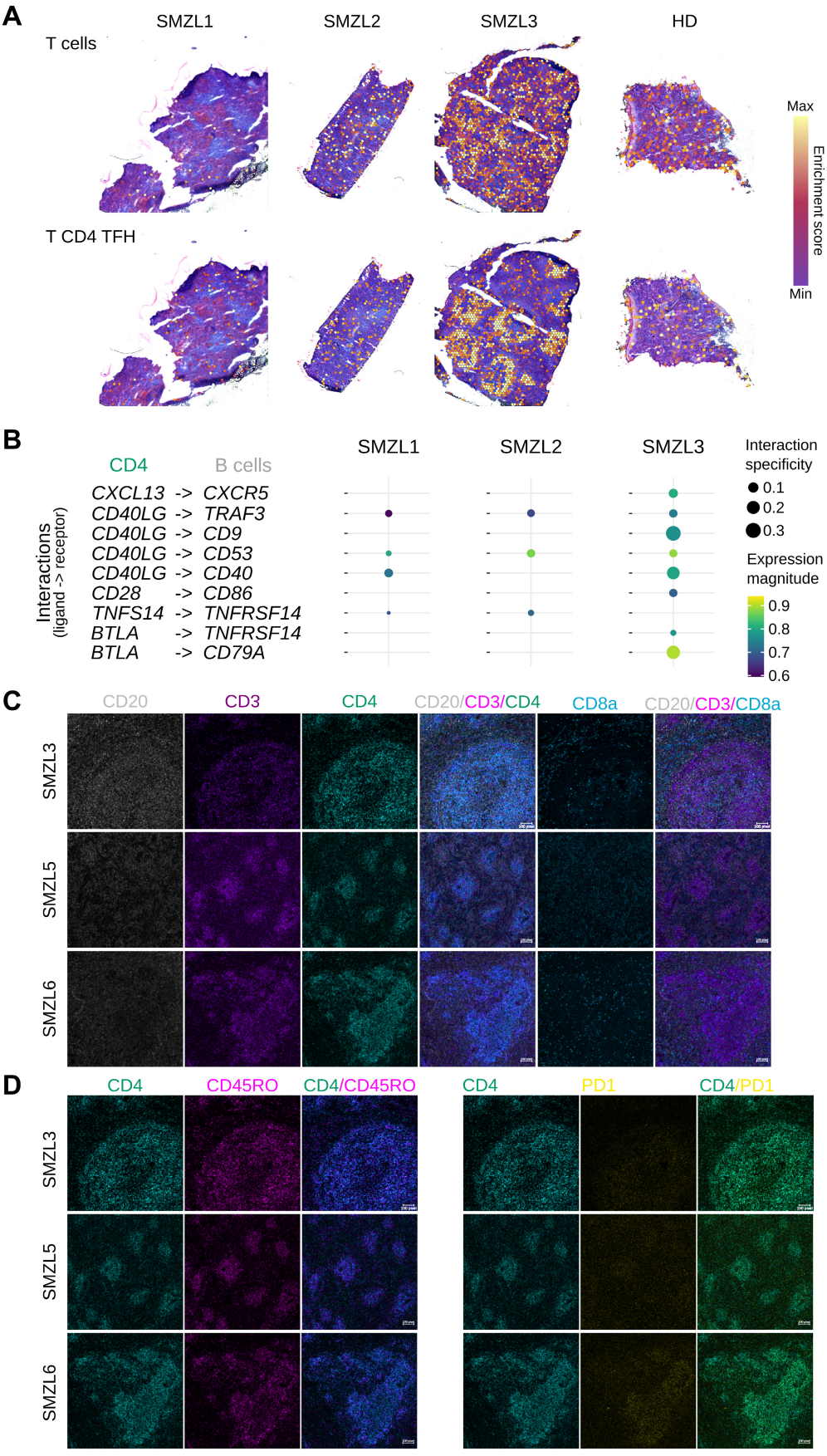

Figure 4. Spatial cartography of immune and tumor B-cell infiltrates in SMZL spleen. (A) T-cell and CD4 T_{FH} infiltrate hallmarks of SMZL splenic tissue and control spleen *in situ* (heatmap of scores for signatures from cell types with transparent background scores in each patient and HD). (B) Ligand–receptor interactions between $CD4^+$ T-cells and tumor B-cells modelized using the LIANA algorithm. (C) IMC (Hyperion) of FFPE SMZL3, SMZL5, and SMZL6 revealing the composition and phenotype of TILs, and (D) revealing T_{FH} cells.

assessed or monitored in blood samples. *In situ* mapping of SMZLs showed distinct patterns of T-cell infiltration, generating neighborhood patterns and specific cell–cell interactions. Together, these findings raise several comments.

First, spatial transcriptomics and multispectral imaging confirmed distinct nodular and diffuse histological patterns of SMZL, at both molecular and phenotypic levels [1,2,15]. Indeed, although BCR signaling as well as NF-kB and NOTCH signaling were enriched in both SMZL subtypes, as reported in bulk samples [12], single-cell data revealed different ranges of expression in cancer cells at the single-cell level. Particularly, the nodular subtype showed a higher BCR signaling score of SMZL tumor cells as compared with diffuse SMZL. The nodular subtype also showed different immune cell compositions and functional states of T-cells in spleen and exhibited the highest density of immune infiltrate. Moreover, several features of the B-cell surrounding T_{FH} in the nodular pattern suggest a critical and possibly more general role of T_{FH} in SMZL disease, as reported in diffuse large B cell lymphoma (DLBCL) and FL [30]. In particular, dynamic interactions between T_{FH} and tumor cells have been shown to sustain B-cell survival and proliferation *in vitro* and *in vivo* [30–33]. A recent study has shown that $PD1^+$ T-cells infiltrating SMZL were more often found near $Ki\text{-}67^+$ proliferating tumor B-cells [34]. Finally, a recent single-cell mass cytometry-based study demonstrated that the presence of T_{FH} was significantly correlated with a higher number of tumor B-cells in SMZL [35]. In our study, spatial transcriptomics and IMC analyses confirmed this close association and unveiled specific gene interactions between T_{FH} subpopulations and tumor B-cells, supporting the key role of T_{FH} in SMZL pathogenesis.

Second, the projection of immune single cells from a newer dataset on a predefined differentiation trajectory (e.g. already built from any public dataset) is highly powerful to precisely characterize their differentiation stage [19,23,36,37]. However, the differentiation trajectory approach in cancer cells represents a major challenge in lymphoma, as their maturation stage mapping is unknown. The present study mapped hyperexpanded SMZL B-cell clones from all patient spleens as $B_{GC\text{-}LZ}$ at Mem-like state, whereas their circulating compartment presented multiple stages of differentiation. Hence, SMZL is not blocked in a specific B-cell state and rather displays a transcriptional desynchronization of B-cell differentiation programs, whatever the patient. The dynamics and plasticity of tumor B-cells, previously discovered in FL, may increase the intra-tumor heterogeneity of SMZL [12,25,31] and thus contribute to the dynamic evolution of the disease.

Third, a recent study revealed that SMZL spleens were infiltrated mainly by exhausted and late-stage differentiated $CD8^+$ T-cells [35]. In our case, 3' and 5' data confirmed these findings, but also extended them thanks to the in-depth exploration of the blood compartment associated with tumor samples. This analysis revealed a similar proportion of T-cell subpopulations in both spleen and its blood counterpart in each patient, but specific differentiation stage. Moreover, the percentage of recirculating TIL clonotypes was variable among patients. The diversity of the TCR repertoire may reflect distinct activation and response of T-cells in patients [38,39]. Some studies have reported that more diverse TCR repertoires in the tumor site as compared with normal tissue are associated with a better prognosis of the disease [40,41]. In addition, a higher number of shared TCR sequences between the tumor and the normal counterpart tissues was also associated with a better outcome [42]. For instance, in DLBCL patients, highly dominant T-cell clonal expansions within the TME are conversely associated with a poor outcome [43], suggesting that genetic diversification of B-cell tumors leads to inadequate immunosurveillance to target all malignant B-cell subclones. However, BCR clonality in SMZL cells is less diverse [6,44]. Indeed, hyperexpanded B-cell clones from SMZL showed a stereotyped IGH CDR3 and were also present in the peripheral blood [44]. Whether the TCR repertoire is associated with good prognosis in SMZL has to be defined in larger series. In conclusion, our integrative phenotypic and transcriptomic analyses at the single-cell level revealed that SMZL tumor B-cells are a patient-specific clonotype expansion, with desynchronized maturation programs. In addition, spatial transcriptomics and mass cytometry revealed the different immune repertoires and infiltrate patterns that are involved in the dynamic ecosystem of SMZL.

Acknowledgements

We acknowledge CRCT and IUCT-O colleagues for their helpful discussions. This work was granted access to the HPC resources of the CALMIP supercomputing center under the allocation 2020-T19001. We are also grateful to the Genotoul bioinformatics platform (Bioinfo Genotoul, Toulouse Midi-Pyrenees) for providing computing resources. This work was supported by grants from the Laboratoire d'Excellence Toulouse Cancer (TOUCAN-2, contract ANR11-LABX), Institut Carnot Lymphome (CALYM), and Ligue Régionale contre le Cancer. We are also grateful to the following for their contribution to this work: Emeline Sarot from the Genomic-Transcriptomic Platform of CRCT, Laetitia Ligat from the Imaging Platform of CRCT, Frederic Pont and Marion Perrier from the Bioinformatic Platform of CRCT, and François-Xavier Frénois from the Imaging Platform of IUCT. PG is supported by the CeVi_Collection project, from the CALYM Carnot Institute, funded by the French National Research Council (ANR). We would like to thank all the members of the spatial imaging mass cytometry and transcriptomics facility (SIMCaT, IRCM, ICM, Montpellier) for the mass cytometry experiment. JPC was supported by ITMO Cancer of the French National Alliance for Life Sciences and Health (Aviesan) and the French National

Cancer Institute (INCa) on funds administered by the French National Institute of Health and Medical Research (Inserm), grant agreement 21CD025-00. We also thank Stéphane Bertani for the proofreading and valuable contribution to this work, and Marie Tosolini for her contribution on the neighboring analysis.

Author contributions statement

CL and J-JF conceived and designed the study. AT-G, LY and CS provided the patient data and samples for this study. PG prepared samples and produced original scRNA-seq and spatial transcriptomic data. JPC conceived the methods, processed and performed bioinformatic data analyses, and generated figures. FM and CV produced original scRNA-seq and spatial transcriptomic data. PB and D-MF provided valuable discussions. CL, J-JF, JPC, PG and AQ-M contributed to data interpretation and writing of the manuscript.

Data availability statement

The raw data produced in this study are available at Gene Expression Omnibus (GEO) with accession number GSE175785, GSE227833, and GSE228056. Published scRNA-seq datasets used in this study are available at the Array Express Archive and GEO with the accession number E-MTAB-9544 [17] and GSE139891 [22], respectively. The references trajectory of γδ T and T CD8 have already been published [19]. Code availability: Seurat is available at the Comprehensive R Archive Network (CRAN) and further details can be found at: https://satijalab.org/seurat/. The collection of R packages (dyno v0.1.2, tidyverse v1.3.0, and Injector) are available from Github via devtools; further details can be found at: https://dynverse.org/ and https://github.com/jp089/single_cell_Injection. Single-Cell Signature Scorer and Single-Cell Virtual Cytometer are available at: https://sites.google.com/site/fredsoftwares/products. Single-cell Multilayer Viewer (scMLV) is available into the GitHub repository at: https://github.com/MarionPerrier/scMLV. Further information and requests for resources and reagents should be directed to and will be fulfilled upon reasonable requests by the Lead Contact, CL (laurent.c@chu-toulouse.fr).

References

1. Campo E, Jaffe ES, Cook JR, *et al*. The international consensus classification of mature lymphoid neoplasms: a report from the clinical advisory committee. *Blood* 2022; **140:** 1229–1253.
2. Alaggio R, Amador C, Anagnostopoulos I, *et al*. The 5th edition of the World Health Organization classification of haematolymphoid tumours: lymphoid neoplasms. *Leukemia* 2022; **36:** 1720–1748.
3. Arcaini L, Rossi D, Paulli M. Splenic marginal zone lymphoma: from genetics to management. *Blood* 2016; **127:** 2072–2081.
4. Thieblemont C. Improved biological insight and influence on management in indolent lymphoma. Talk 3: update on nodal and splenic marginal zone lymphoma. *Hematology Am Soc Hematol Educ Program* 2017; **2017:** 371–378.
5. Broccoli A, Zinzani PL. How do we sequence therapy for marginal zone lymphomas? *Hematology Am Soc Hematol Educ Program* 2020; **2020:** 295–305.
6. Zibellini S, Capello D, Forconi F, *et al*. Stereotyped patterns of B-cell receptor in splenic marginal zone lymphoma. *Haematologica* 2010; **95:** 1792–1796.
7. Bikos V, Darzentas N, Hadzidimitriou A, *et al*. Over 30% of patients with splenic marginal zone lymphoma express the same immunoglobulin heavy variable gene: ontogenetic implications. *Leukemia* 2012; **26:** 1638–1646.
8. Kiel MJ, Velusamy T, Betz BL, *et al*. Whole-genome sequencing identifies recurrent somatic NOTCH2 mutations in splenic marginal zone lymphoma. *J Exp Med* 2012; **209:** 1553–1565.
9. Rossi D, Trifonov V, Fangazio M, *et al*. The coding genome of splenic marginal zone lymphoma: activation of NOTCH2 and other pathways regulating marginal zone development. *J Exp Med* 2012; **209:** 1537–1551.
10. Clipson A, Wang M, de Leval L, *et al*. KLF2 mutation is the most frequent somatic change in splenic marginal zone lymphoma and identifies a subset with distinct genotype. *Leukemia* 2015; **29:** 1177–1185.
11. Piva R, Deaglio S, Famà R, *et al*. The Krüppel-like factor 2 transcription factor gene is recurrently mutated in splenic marginal zone lymphoma. *Leukemia* 2015; **29:** 503–507.
12. Bonfiglio F, Bruscaggin A, Guidetti F, *et al*. Genetic and phenotypic attributes of splenic marginal zone lymphoma. *Blood* 2022; **139:** 733–747.
13. Novak U, Rinaldi A, Kwee I, *et al*. The NF-{kappa}B negative regulator TNFAIP3 (A20) is inactivated by somatic mutations and genomic deletions in marginal zone lymphomas. *Blood* 2009; **113:** 4918–4921.
14. Marmey B, Boix C, Barbaroux J-B, *et al*. CD14 and CD169 expression in human lymph nodes and spleen: specific expansion of CD14+CD169− monocyte-derived cells in diffuse large B-cell lymphomas. *Hum Pathol* 2006; **37:** 68–77.
15. Laurent C, Cook JR, Yoshino T, *et al*. Follicular lymphoma and marginal zone lymphoma: how many diseases? *Virchows Arch* 2023; **482:** 149–162.
16. Laurent C, Adélaïde J, Guille A, *et al*. High-grade follicular lymphomas exhibit clinicopathologic, cytogenetic, and molecular diversity extending beyond grades 3A and 3B. *Am J Surg Pathol* 2021; **45:** 1324–1336.
17. Stewart A, Ng JC-F, Wallis G, *et al*. Single-cell transcriptomic analyses define distinct peripheral B cell subsets and discrete development pathways. *Front Immunol* 2021; **12:** 602539.
18. Pont F, Tosolini M, Fournié JJ. Single-cell signature explorer for comprehensive visualization of single cell signatures across scRNA-seq datasets. *Nucleic Acids Res* 2019; **47:** e133.
19. Cerapio J-P, Perrier M, Balança C-C, *et al*. Phased differentiation of γδ T and T CD8 tumor-infiltrating lymphocytes revealed by single-cell transcriptomics of human cancers. *OncoImmunology* 2021; **10:** 1939518.
20. Pont F, Cerapio JP, Gravelle P, *et al*. Single-cell spatial explorer: easy exploration of spatial and multimodal transcriptomics. *BMC Bioinformatics* 2023; **24:** 30.
21. Saelens W, Cannoodt R, Todorov H, *et al*. A comparison of single-cell trajectory inference methods. *Nat Biotechnol* 2019; **37:** 547–554.
22. Holmes AB, Corinaldesi C, Shen Q, *et al*. Single-cell analysis of germinal-center B cells informs on lymphoma cell of origin and outcome. *J Exp Med.* 2020; **217:** e20200483.

23. Cerapio JP, Perrier M, Pont F, *et al*. Single-cell RNAseq profiling of human γδ T lymphocytes in virus-related cancers and COVID-19 disease. *Viruses* 2021; **13:** 2212.
24. Cano-Gamez E, Soskic B, Roumeliotis TI, *et al*. Single-cell transcriptomics identifies an effectorness gradient shaping the response of CD4+ T cells to cytokines. *Nat Commun* 2020; **11:** 1801.
25. Milpied P, Cervera-Marzal I, Mollichella M-L, *et al*. Human germinal center transcriptional programs are de-synchronized in B cell lymphoma. *Nat Immunol* 2018; **19:** 1013–1024.
26. Ycart B, Pont F, Fournié J-J. Curbing false discovery rates in interpretation of genome-wide expression profiles. *J Biomed Inform* 2014; **47:** 58–61.
27. Dimitrov D, Türei D, Garrido-Rodriguez M, *et al*. Comparison of methods and resources for cell-cell communication inference from single-cell RNA-Seq data. *Nat Commun* 2022; **13:** 3224.
28. Glasson Y, Chépeaux L-A, Dumé A-S, *et al*. Single-cell high-dimensional imaging mass cytometry: one step beyond in oncology. *Semin Immunopathol* 2023; **45:** 17–28.
29. Glasson Y, Chépeaux L-A, Dumé A-S, *et al*. A 31-plex panel for high-dimensional single-cell analysis of murine preclinical models of solid tumors by imaging mass cytometry. *Front Immunol* 2023; **13:** 1011617.
30. Mintz MA, Cyster JG. T follicular helper cells in germinal center B cell selection and lymphomagenesis. *Immunol Rev* 2020; **296:** 48–61.
31. Attaf N, Dong C, Gil L, *et al*. Functional plasticity and recurrent cell states of malignant B cells in follicular lymphoma. *bioRxiv* 2022; https://doi.org/10.1101/2022.04.06.487285. [Not peer reviewed].
32. Iqbal J, Meyer PN, Smith LM, *et al*. BCL2 predicts survival in germinal center B-cell-like diffuse large B-cell lymphoma treated with CHOP-like therapy and rituximab. *Clin Cancer Res* 2011; **17:** 7785–7795.
33. Cha Z, Guo H, Tu X, *et al*. Alterations of circulating follicular helper T cells and interleukin 21 in diffuse large B-cell lymphoma. *Tumor Biol* 2014; **35:** 7541–7546.
34. Wickenden K, Nawaz N, Mamand S, *et al*. PD1^{hi} cells associate with clusters of proliferating B-cells in marginal zone lymphoma. *Diagn Pathol* 2018; **13:** 74.
35. Anagnostou T, Yang Z-Z, Jalali S, *et al*. Characterization of immune exhaustion and suppression in the tumor microenvironment of splenic marginal zone lymphoma. *Leukemia* 2023; **37:** 1485–1498.
36. Cerapio J, Perrier M, Pont F, *et al*. Single-cell differentiation trajectories define early stages of a human cutaneous T-cell lymphoma. *Explor Immunol* 2022; **2:** 185–199.
37. Trapnell C, Cacchiarelli D, Grimsby J, *et al*. The dynamics and regulators of cell fate decisions are revealed by pseudotemporal ordering of single cells. *Nat Biotechnol* 2014; **32:** 381–386.
38. Porciello N, Franzese O, D'Ambrosio L, *et al*. T-cell repertoire diversity: friend or foe for protective antitumor response? *J Exp Clin Cancer Res* 2022; **41:** 356.
39. Hosoi A, Takeda K, Nagaoka K, *et al*. Increased diversity with reduced "diversity evenness" of tumor infiltrating T-cells for the successful cancer immunotherapy. *Sci Rep* 2018; **8:** 1058.
40. Valpione S, Mundra PA, Galvani E, *et al*. The T cell receptor repertoire of tumor infiltrating T cells is predictive and prognostic for cancer survival. *Nat Commun* 2021; **12:** 4098.
41. Aran A, Garrigós L, Curigliano G, *et al*. Evaluation of the TCR repertoire as a predictive and prognostic biomarker in cancer: diversity or clonality? *Cancers (Basel)* 2022; **14:** 1771.
42. Wang X, Zhang B, Yang Y, *et al*. Characterization of distinct T cell receptor repertoires in tumor and distant non-tumor tissues from lung cancer patients. *Genomics Proteomics Bioinformatics* 2019; **17:** 287–296.
43. Keane E, Francis EC, Catháin ÉÓ, *et al*. The role of race in thyroid cancer: systematic review. *J Laryngol Otol* 2017; **131:** 480–486.
44. Bagnara D, Colombo M, Reverberi D, *et al*. Characterizing features of human circulating B cells carrying CLL-like stereotyped immunoglobulin rearrangements. *Front Oncol* 2022; **12:** 894419.
45. Chihara N, Madi A, Kondo T, *et al*. Induction and transcriptional regulation of the co-inhibitory gene module in T cells. *Nature* 2018; **558:** 454–459.
46. Butler A, Hoffman P, Smibert P, *et al*. Integrating single-cell transcriptomic data across different conditions, technologies, and species. *Nat Biotechnol* 2018; **36:** 411–420.
47. Stuart T, Butler A, Hoffman P, *et al*. Comprehensive integration of single-cell data. *Cell* 2019; **177:** 1888–1902.e21.
48. Victora GD, Dominguez-Sola D, Holmes AB, *et al*. Identification of human germinal center light and dark zone cells and their relationship to human B-cell lymphomas. *Blood* 2012; **120:** 2240–2248.
49. Zanotelli VR, Bodenmiller B. mcSegmentationPipeline: a pixelclassification based multiplexed image segmentation pipeline. *Zenodo*. Available from: https://doi.org/10.5281/zenodo.3841961.

References 46–49 are cited only in the supplementary material.

SUPPLEMENTARY MATERIAL ONLINE

Supplementary materials and methods

Figure S1. Integration of 3' and 5' datasets

Figure S2. Reference trajectory of peripheral B-cell differentiation

Figure S3. Reference trajectory of B_{GC} differentiation

Figure S4. Reference trajectory of CD4 T-cell differentiation

Figure S5. Spatial transcriptomics of SMZL tumors

Figure S6. IMC neighborhood analysis and association between T_{FH} and tumor B-cell proliferation

Table S1. Hyperion antibody panel